

Multi-component colloidal gels: interplay between structure and mechanical proprieties (Supplementary Information)

1 Dependence of pore size on concentration

As was mentioned in the main text, the pore size (at the same total concentration) is similar in monogels, bi-gels and tri-gels. In fact, there is a dependence of the average pore size ($\langle \ell/d \rangle$) with packing fraction that behaves as $\langle \ell/d \rangle \propto 1/\phi$ in the three cases. Figure 1 shows this dependence.

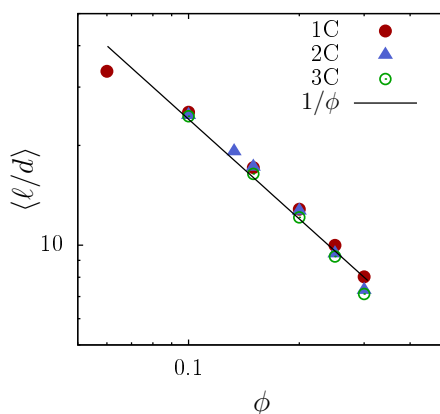


Figure 1: Dependence of the average chord length $\langle \ell/d \rangle$ on the packing fraction ϕ .

2 Bond autocorrelation during deformation

Fig. 5a in the main text, shows how there is a bigger and faster increment of the bonds for monogels during deformation than in the other two cases. In fact, for multi-gels, more particles that were bonded at the beginning of the deformation are bonded later on than in the monogel case. To quantify the amount of change in the gel network, we calculated

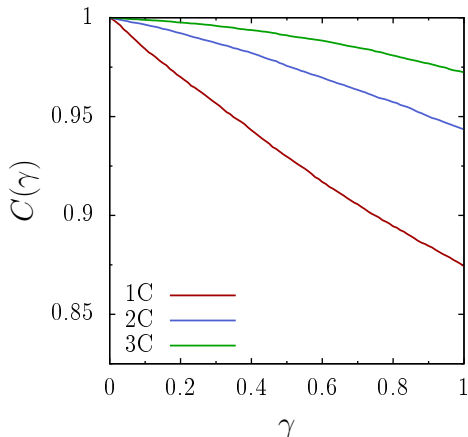


Figure 2: Bond autocorrelation $C(\gamma)$ as a function of deformation γ . The three systems are at the same total packing fraction $\phi_{tot} = 0.20$.

the bond autocorrelation function. We define the bond autocorrelation function $C(\gamma)$ at each deformation step γ as,[?]

$$C(\gamma) = \frac{\langle \sum_{i<j} c_{ij}(0)c_{ij}(\gamma) \rangle}{\langle \sum_{i<j} c_{ij}^2(0) \rangle}. \quad (1)$$

Where $c_{ij}(\gamma)$ is the $N \times N$ matrix that defines the bonds at a deformation γ as,

$$c_{ij}(\gamma) = \begin{cases} 1 & \text{if particles } i \text{ and } j \text{ are bonded} \\ 0 & \text{else} \end{cases}. \quad (2)$$

This quantity measures the amount of change in the bonding pairs between the initial structure and the one at each deformation step. Figure 2 shows $C(\gamma)$ for the three mixtures at a packing fraction of $\phi_{tot} = 0.20$. From this graph, it can be seen that in the monogel the initial bonds disappear faster than in the other two cases. It should be pointed out that this quantity takes into account both, bond breaking and bond reformation. Even so, the changes from the original gel network are bigger in monogels than in multi-gels.

3 Equal relative concentration

Fig. 3 shows the pore chord distribution function for three different multi-gels: 1C at $\phi_{tot} = 0.066$, 2C at $\phi_{tot} = 0.133$ and 3C at $\phi_{tot} = 0.20$. Each system has the same relative concentration for each species, i.e. $\phi_{tot}/m = 0.066$ for $m = 1, 2, 3$. In Fig. 3, a difference in the distribution for big l s can be observed. This comes from the fact, that although the relative packing fraction in the three panels is the same, the total packing fraction in each mixtures is different. For the trigel, the higher total packing

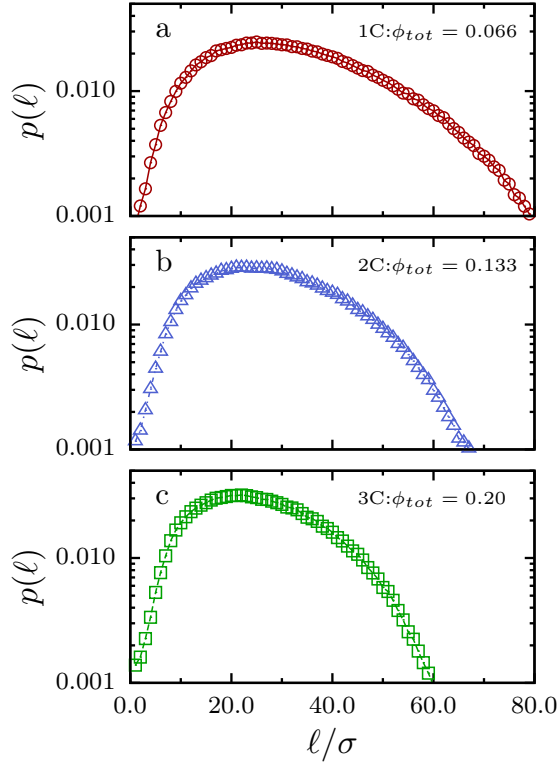


Figure 3: Pore chord length distribution $p(\ell)$ for 1C, 2C and 3C systems with a packing fraction for each species of $\phi_m = \phi_{tot}/m = 0.066$ (i.e. $\phi_1 = \phi_2 = \phi_3$). Data corresponds to the average structure obtained after sample preparation.

fraction restricts the network structure of each species, making the pore tighter than for monogels.

If we analyse the microscopic configuration changes during continuous deformation for each species in Fig. 4 we get a different trend than in Fig. 5 in the main paper. In this case, the rate of increment in the number of bonds for each species is different (Fig. 4a), despite the fact that each species is at the same relative packing fraction. This is given by the difference in total packing fractions and the restrictions bonds connectivity's imposed by the inter-species and intra-species interactions set by Eq. 1-2 in the main paper. Nonetheless, at small strain deformations the squared non affine displacements are similar. This is seen in Fig. 4b, where difference in $\langle \Delta_n^2 \rangle$ are more notorious for $\gamma > 0.1$, where we have left the linear regime. The last panel, Fig. 4c, shows the average pore length. This, as mentioned before, is bigger in the 1C system because of the restrictions imposed by different total packing fractions. The three panels indicate an steric repulsion effect of each species in multi-gels.

Finally, to complete the picture, Fig. 5 shows another interesting feature of multi-gels. If in a gel with m components one of them is melted into a gas, the remaining

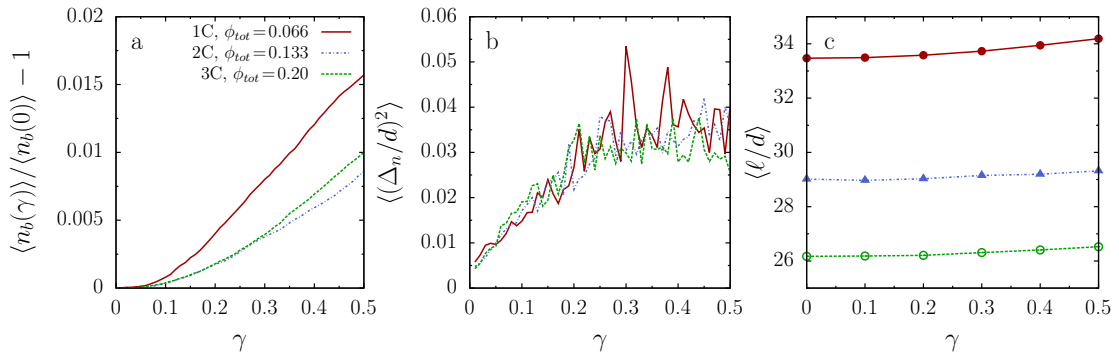


Figure 4: a) Rate of increment of the average number of bonds per particle, per species, during deformation. b) Average non-affine squared displacement per species vs. stress. c) Average ℓ at different strains for each species. All samples are at the same relative packing fraction $\phi_m = \phi_{tot}/m = 0.066$ (i.e. $\phi_1 = \phi_2 = \phi_3$). Analysis for samples under continuous shearing with a strain increment $\Delta\gamma = 0.01$ and shear rate $\dot{\gamma} = 10^{-5}\tau_0^{-1}$.

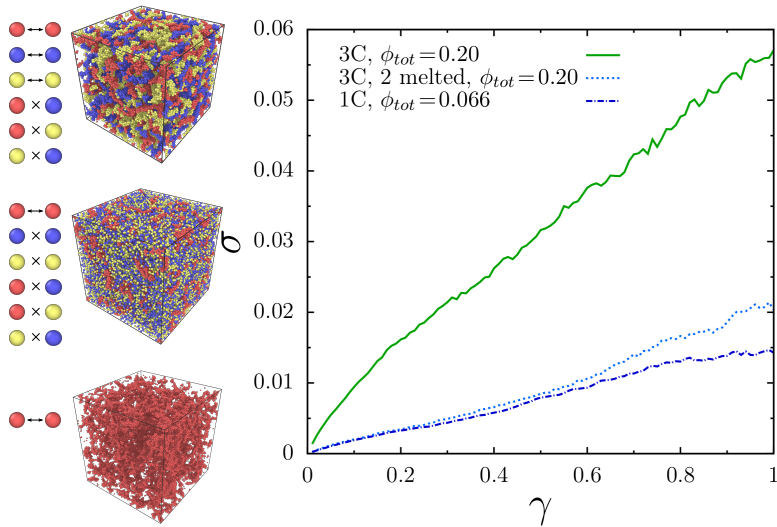


Figure 5: Stress vs. strain curve for fixed component packing fraction $\phi_m = 0.066$ for monogel and trigel. Three different scenarios are shown: trigel at $\phi_{tot} = 0.20$ (green line), trigel with two components melted at $\phi_{tot} = 0.20$ (light blue line) and monogel at $\phi_{tot} = 0.066$ (dark blue line).

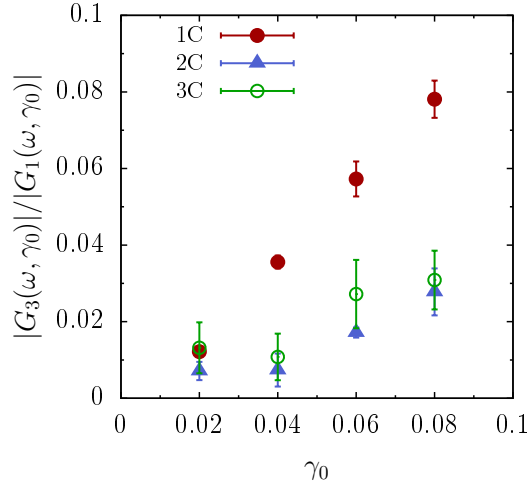


Figure 6: Ratio between the modules of the third and first harmonic terms for the shear stress for maximum strains γ_0 .

network is equivalent to a gel of $m-1$ components at a packing fraction $(m-1)\phi_m$. This is shown in Fig. 5 for a trigel at $\phi_{tot} = 0.20$. When two of the components are melted, we recover a strain-stress curve that is similar to the one of a mono-gel at $\phi_{tot} = 0.066$. A similar trend is found when only one component is melted, and the resulting mixture is compared with a bi-gel at $\phi_{tot} = 0.133$, which is not shown here. This shows that the effect of steric repulsion created by different species is governing the response in multi-gels.

4 More on the extended linear regime in multigels

Figure 3b-d in the main text, show that multi-gels have an extended linear regime compared to monogels. To show this further, we calculated the ratio between the third and first harmonic terms of the shear modulus:

$$|G_3(\omega, \gamma_0)|/|G_1(\omega, \gamma_0)| = \frac{\sqrt{(G'_3(\omega, \gamma_0))^2 + (G''_3(\omega, \gamma_0))^2}}{\sqrt{(G'_1(\omega, \gamma_0))^2 + (G''_1(\omega, \gamma_0))^2}}. \quad (3)$$

Figure 6 shows the ratios $|G_3(\omega, \gamma_0)|/|G_1(\omega, \gamma_0)|$ obtained from oscillatory rheology for different maximum strains values in the range $0.2 \leq \gamma_0 \leq 0.08$. For all the cases an equivalent shear ratio of $\omega\gamma_0 = 10^{-5}\tau_0^{-1}$ was kept. The points for $\gamma_0 = 0.08$ correspond to the curves reported in Figure 3b-d. This graph corroborates what is already mentioned in the main text, the extended linearity in the case of multi-gels.

5 Linear oscillatory response at vanishing frequency

In our multi-gels, the linear oscillatory response in a frequency sweep for sufficiently small frequencies $\omega\tau_0$ gives $G' \gg G''$. Fig. 7, shows the oscillatory response for small deformations $\gamma_0 = 0.01$ for multi-gels at packing fractions $\phi_{tot} = 0.10$ and $\phi_{tot} = 0.30$. There, it can be seen that $G' \gg G''$ and that G' approaches a constant value G_0 for small frequencies. All the G_0 values reported in the main paper were obtained from frequencies values $\omega\tau_0 \leq 10^{-4}$, where we approach constant values, as shown in Fig. 7.

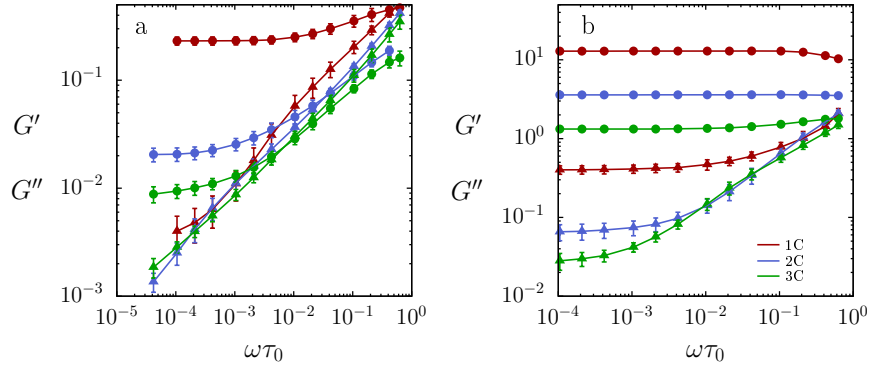


Figure 7: Oscillatory response G' (circles) and G'' (triangles) for small deformations $\gamma_0 = 0.01$ as a function of frequency $\omega\tau_0$. Data for 1C, 2C and 3C systems at packing fractions a) $\phi_{tot} = 0.10$ and b) $\phi_{tot} = 0.30$.